RSC Advances

PAPER

View Article Online
View Journal | View Issue

Cite this: *RSC Adv.*, 2020, **10**, 33026

The *in situ* preparation of iron phosphide using ionic liquids as iron and phosphorus sources for efficient hydrogen evolution reactions†

Yanping Chen,[ab] Tianhao Li,[ab]* Qichao Zhao,[c] Dingyu Liu[ab] and Chang Ming Li[ab]

Ionic liquids (ILs) were utilized as iron and phosphorus sources for the preparation of iron phosphide for the first time. The IL trihexyl(tetradecyl)phosphonium tetrachloroferrate ($[P(C_6H_{13})_3C_{14}H_{29}][FeCl_4]$) and carbon nanotubes (CNTs) were applied as precursors for the *in situ* preparation of $Fe_2P_{(IL6)}$/CNTs. This material has good catalytic activity and stability for the hydrogen evolution reaction, including a low onset overpotential (75 mV) and Tafel slope (68 mV dec^{-1}). Moreover, this catalyst exhibits current densities of 10 and 20 mA cm^{-2} at overpotentials of 115 and 150 mV, respectively. The phosphidation process using $[P(C_6H_{13})_3C_{14}H_{29}][FeCl_4]$ was also investigated. All experimental results indicate that Fe_2P can be formed *in situ* on the CNTs using this IL, and that the CNTs help the formation of the Fe_2P nanoparticles and improve the electrical conductivity. This IL-based *in situ* preparation strategy is facile and environmentally friendly and does not require the addition of other reagents. This method holds great promise for application in other electrochemical studies.

Received 29th June 2020
Accepted 22nd August 2020

DOI: 10.1039/d0ra05666a

rsc.li/rsc-advances

Introduction

Due to the environmental impact of fossil fuels and the energy crisis, the development of some clean, low-carbon emission, renewable and efficient energy sources to replace fossil fuels is required. Hydrogen is a sustainable and green energy source and a carrier with a high energy density, which could enable the world to meet future energy demand. Water electrolysis is a simple and reliable method to generate H_2 without carbon emissions and normally needs a high overpotential.[1] In order to decrease the required overpotential and to increase the current density, electrocatalysts for the hydrogen evolution reaction (HER) are highly desired. Noble metal-based catalysts have excellent HER activities but their high price and low abundance have restricted their practical application.[2] Also, the proton exchange membrane used for water splitting demands that the HER electrocatalyst is acid-stable.[3] Thus, it is necessary to develop some inexpensive, stable and highly efficient catalysts for the HER.[4] Recently, transition metal phosphides (TMPs) have been introduced as a promising catalyst material due to their low-cost, good catalytic efficiency and stability.[5] Various kinds of TMPs have been prepared as electrocatalysts for the HER, such as MoP, WP, NiP, FeP and CoP.[6–11] Amongst the transition metals, iron is the cheapest and most abundant, so iron phosphide-based catalysts, including FeP, Fe_2P, Fe_3P and FeMnP, have been introduced and widely applied in the HER.[12–14] To prepare iron phosphide, different iron salts (*e.g.* $FeCl_3$ and $FeSO_4$) and phosphorus compounds (*e.g.* trioctylphosphine and NaH_2PO_2) have frequently been used as the Fe and P sources, respectively.[12–17] However, some of these preparation methods have adopted complicated procedures to obtain a good HER performance.[6,12–17] Hence, it is vital to develop a simple approach to the synthesis of iron phosphide with novel Fe and P sources.

Ionic liquids (ILs) are organic molten salts that possess low melting points (<100 °C). Various ILs have been applied in the HER due to their high conductivities and stabilities.[18–20] In our previous study, an IL with a tetrachloroferrate anion was synthesized and applied as the iron source to prepare FeP for use in the HER. The resulting FeP showed good catalytic activity.[21] However, this synthetic process is tedious and time consuming, and an additional P source is needed for the preparation of FeP. Thus, it is essential to use some novel metal and phosphorus sources to simplify the preparation route. In this study, an *in situ* iron phosphide preparation method was developed, where ILs containing a phosphonium cation and a tetrachloroferrate anion were utilized as a dual iron and phosphorus source for the first time. Generally, trihexyl(tetradecyl)phosphonium tetrachloroferrate ($[P(C_6H_{13})_3C_{14}H_{29}]$

[a]School of Materials and Energy, Southwest University, Chongqing 400715, China. E-mail: tli7@swu.edu.cn
[b]Chongqing Key Laboratory for Advanced Materials and Technologies of Clean Energy, Chongqing 400715, China
[c]Bureau of Hydrology, Changjiang Water Resources Commission, Wuhan 430010, China

† Electronic supplementary information (ESI) available. See DOI: 10.1039/d0ra05666a

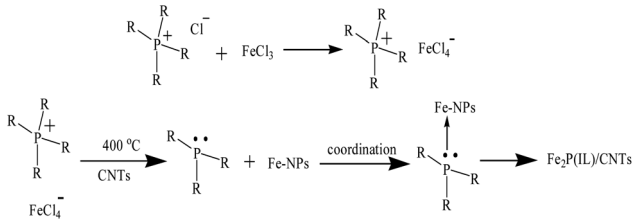

Scheme 1 The preparation of $Fe_2P_{(IL4)}$/CNTs and $Fe_2P_{(IL6)}$/CNTs.

$[FeCl_4]$) and tetrabutylphosphonium tetrachloroferrate ($[P(C_4H_9)_4][FeCl_4]$) were quickly synthesized, and then these two ILs were mixed with carbon nanotubes (CNTs) to prepare the $Fe_2P_{(IL6)}$/CNTs and $Fe_2P_{(IL4)}$/CNTs materials *via* low temperature pyrolysis (Scheme 1). These as-prepared iron phosphides exhibited good HER activity and stability. During the preparation, the CNTs facilitated the formation of the Fe_2P nanoparticles as well as improving the conductivity of these catalysts. This IL-based *in situ* preparation strategy is uncomplicated, quick, and environmentally friendly without needing the addition of other organic solvents and harmful reagents. It holds great promise for applications in other electrochemical studies.

Experimental

Chemicals

Trihexyl(tetradecyl)phosphonium chloride ($[P(C_6H_{13})_3C_{14}H_{29}][Cl]$), tetrabutylphosphonium chloride ($[P(C_4H_9)_4][Cl]$), iron(III) chloride hexahydrate ($FeCl_3 \cdot 6H_2O$) and other reagents were purchased from Titansci Co. China. Multi-walled carbon nanotubes (CNTs) were supplied by Shenzhen Nanotech Port Ltd, Co. China.

Synthesis of ionic liquids and the preparation of Fe_2P

Two ionic liquids (ILs), namely trihexyl(tetradecyl)phosphonium tetrachloroferrate ($[P(C_6H_{13})_3C_{14}H_{29}][FeCl_4]$) and tetrabutylphosphonium tetrachloroferrate ($[P(C_4H_9)_4][FeCl_4]$), were synthesized *via* a previously reported procedure.[22] Generally, $[P(C_6H_{13})_3C_{14}H_{29}][Cl]$ was mixed with $FeCl_3 \cdot 6H_2O$ in methanol for 24 h at room temperature and the dark red product was automatically separated from the solvent. After removing the solvent, the homogeneous product was dried under vacuum to afford $[P(C_6H_{13})_3C_{14}H_{29}][FeCl_4]$. Then, this IL was mixed with CNTs in a mortar to obtain a IL6/CNTs mixture, which was subsequently pyrolyzed in a tube furnace for *in situ* preparation of $Fe_2P_{(IL6)}$/CNTs (400 °C in an Ar atmosphere for 2 h) (Scheme 1). Similarly, $[P(C_4H_9)_4][Cl]$ was reacted with $FeCl_3 \cdot 6H_2O$ to synthesize $[P(C_4H_9)_4][FeCl_4]$, which was further mixed with CNTs and pyrolyzed to obtain $Fe_2P_{(IL4)}$/CNTs. For comparison, $[P(C_6H_{13})_3C_{14}H_{29}][FeCl_4]$ was directly pyrolyzed without CNTs to prepare $Fe_2P_{(IL6)}$ under the same conditions. $FeCl_3 \cdot 6H_2O$ was mixed with CNTs and sodium hypophosphite (NaH_2PO_2) and was then pyrolyzed to prepare FeP/CNTs under the same conditions.

Electrocatalytic performance

All electrochemical measurements were conducted on an electrochemical workstation (CHI-760E) with a three-electrode configuration at ambient temperature, where a glassy carbon electrode (GCE, 0.126 cm^2), a carbon rod and a saturated calomel electrode (SCE) were employed as the working electrode, the counter electrode and the reference electrode in 0.5 M H_2SO_4, respectively. 10 μL of a catalyst ethanol solution (5 mg ml^{-1}) with Nafion (5 wt%) was dropped on the clean GCE and dried to prepare the working electrode. For each analysis, the measurement was repeated at least three times. The linear sweep voltammograms (LSV) were performed at a scan rate of 2 mV s^{-1} (from 0.2 to −1 V). The electrochemical impedance spectroscopy (EIS) measurements of the catalysts were recorded at −400 mV over a frequency range of 0.1–1000 kHz with a 5 mA amplitude of current perturbation.

Characterization

The morphology and structure of the material were studied using field emission scanning electron microscopy (FE-SEM, JEOL-7800F), transmission electron microscopy (TEM, JEM-2100) and energy dispersive X-ray spectroscopy (EDX, INCA X-Max 250). The measurement of the X-ray diffraction (XRD) patterns was conducted using a RigakuD/Max 2550 diffractometer with Cu Kα radiation ($\lambda = 1.5418$ Å). X-ray photoelectron spectroscopy (XPS) characterization was performed using a ESCALAB 250Xi spectrometer with Al Kα (150 W, 1486.6 eV) radiation. The specific surface area was analyzed using a nitrogen adsorption method (BET method) through a TriStar II 3020 gas sorption analyzer.

Results and discussion

The morphology of the $Fe_2P_{(IL6)}$/CNTs was examined using FE-SEM and TEM. As shown in Fig. 1 and S1 in the ESI,† Fe_2P was uniformly generated *in situ* on the CNTs. These Fe_2P nanoparticles are sphere-shaped with a diameter of approximately 40–70 nm. These images clearly illustrate that the Fe_2P nanospheres are wrapped in the CNTs. Moreover, a size distribution histogram based on the TEM images was obtained (Fig. S2†), showing that the diameters of the particles almost ranged from 40–60 nm. The energy dispersive spectroscopy (EDS) analysis reveals that C, O, P and Fe are the main elements of $Fe_2P_{(IL6)}$/CNTs. The EDS mapping results indicate that the Fe and P are evenly spread on the CNTs (Fig. 2 and S3†). It also suggests that during the preparation, the CNTs uniformly disperse the $[P(C_6H_{13})_3C_{14}H_{29}][FeCl_4]$ for *in situ* formation of the Fe_2P nanospheres. Furthermore, the EDS pattern (Fig. 2a) shows that the atomic percentage of Fe and P in $Fe_2P_{(IL6)}$/CNTs was 36.6 and 18.35%, respectively. These results indicate that the Fe and P molar ratio in the catalyst is 2 : 1, yet this ratio is 1 : 1 in the $[P(C_6H_{13})_3C_{14}H_{29}][FeCl_4]$ IL. A possible reason for this change in the Fe : P ratio could be that during the preparation process (Scheme 1) some of the phosphorus formed may react with other atoms (such as Cl and H) to form volatiles that are transferred out of the tube furnace by the carrier gas (Ar).

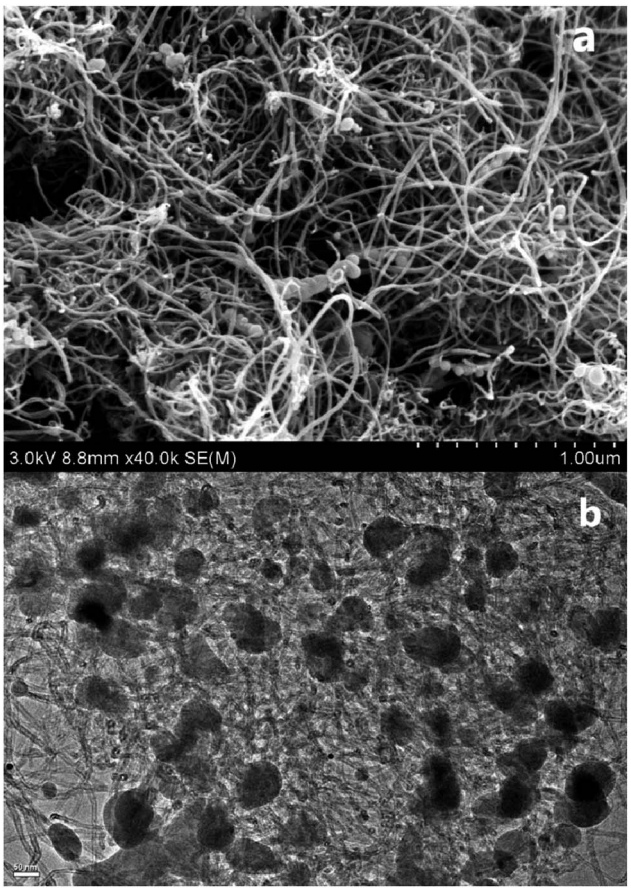

Fig. 1 (a) An SEM image of $Fe_2P_{(IL6)}$/CNTs; and (b) a TEM image of $Fe_2P_{(IL6)}$/CNTs (scale bar: 50 nm).

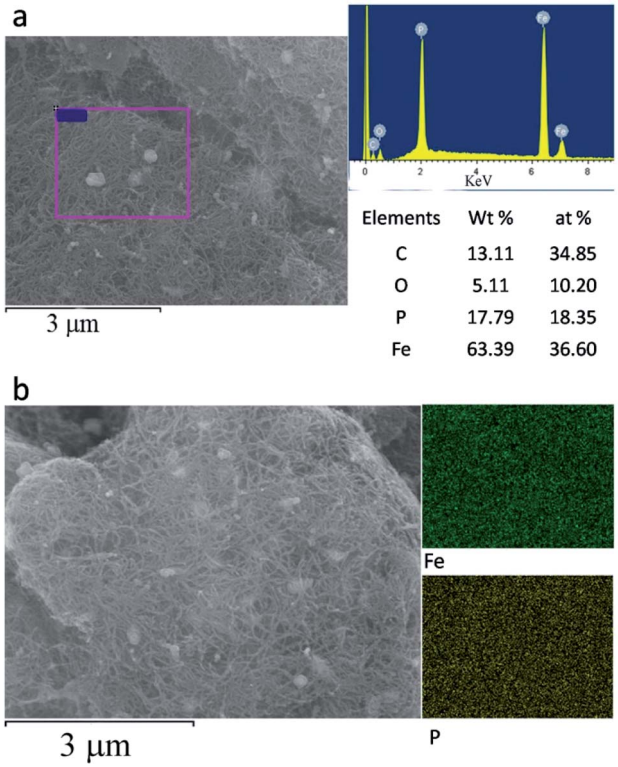

Fig. 2 (a) The EDS pattern of $Fe_2P_{(IL6)}$/CNTs; and (b): EDS mapping of Fe and P in $Fe_2P_{(IL6)}$/CNTs.

Moreover, this change in stoichiometric ratio preliminarily demonstrates the formation of Fe_2P. For comparison, SEM, TEM and EDS analyses were also performed for $Fe_2P_{(IL4)}$/CNTs, FeP/CNTs and $Fe_2P_{(IL6)}$. As shown in Fig. 1, 2 and S4–S6,† $Fe_2P_{(IL6)}$/CNTs has a smaller particle size and a higher Fe_2P content than $Fe_2P_{(IL4)}$/CNTs and FeP/CNTs. The FeP/CNTs nanoparticles were aggregated and the $Fe_2P_{(IL6)}$ sample has a large sheet morphology.

In addition, XRD and XPS characterizations of $Fe_2P_{(IL6)}$/CNTs were carried out to further confirm the formation of Fe_2P. The broad peak in the XRD pattern from 20 to 28° can be assigned to the presence of CNTs in this material. The XRD pattern of $Fe_2P_{(IL6)}$/CNTs displayed characteristic diffraction peaks at 40.4° (111), 44.2° (201), 47.3° (210), 52.9° (002), 54.1° (300), 54.6° (211), 73.6° (212) and 79.1° (302), which is in agreement with the Fe_2P reference pattern (PDF#51-0943) (Fig. 3).[23] The small positive shift of the $Fe_2P_{(IL6)}$/CNTs peaks may result from the oxygen dopant observed in the EDS data.[10] Some of the iron could be oxidized during the phosphidation and so the unidentified peak around 43° may be attributed to the iron oxidized species. A Scherrer analysis of the XRD data was conducted, and the results indicated that the average grain size is 52.7 nm (Fig. S2†), which is in accordance with the TEM data. Bonding information relating to $Fe_2P_{(IL6)}$/CNTs was investigated through XPS analysis. In the Fe 2p spectrum (Fig. 4a) two broad peaks were observed at binding energies (BEs) of 712.6 eV and 726.7 eV. These are most likely related to the amorphous iron oxide species (Fe–O) in the material, indicating that the Fe^{3+} was not totally reduced to a zero valence state.[24] Two sharp peaks were found at 707.5 eV (Fe $2p_{3/2}$) and 720.3 eV (Fe $2p_{1/2}$). Also, the P 2p spectrum reveals two peaks located at 129.4 eV (P $2p_{3/2}$) and 130.1 eV (P $2p_{1/2}$). The Fe $2p_{3/2}$ peak (707.5 eV) is a little higher than that of elemental Fe (707.0 eV) while the P $2p_{3/2}$ peak (129.4 eV) is a little lower than that of elemental P (130.2 eV), which is consistent with the structure of Fe_2P.[25–27] Also, it suggests that electrons were transferred from iron to phosphorus, where Fe and P have a partial positive charge (δ+) and

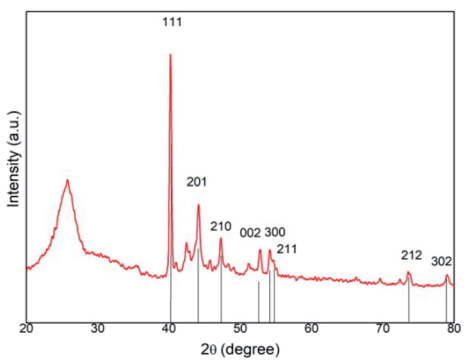

Fig. 3 The XRD pattern of $Fe_2P_{(IL6)}$/CNTs.

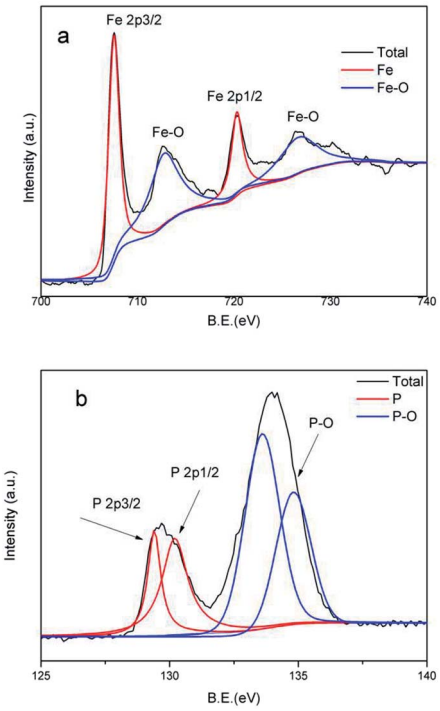

Fig. 4 (a) The Fe 2p XPS spectrum of $Fe_2P_{(IL6)}$/CNTs; and (b) the P 2p XPS spectrum of $Fe_2P_{(IL6)}$/CNTs.

a partial negative charge ($\delta-$), respectively.[28,29] Another peak located at 133.9 eV may arise from the oxidized P species, suggesting the formation of phosphorous based oxides (Fig. 4b).[28,29] The existence of oxidized Fe and P can be assumed to arise from the surface oxidation of Fe_2P under ambient conditions.[28] In addition, the relative area ratio of the P 2p peak area at 133.9 eV is higher than that of the other P 2p peaks. Its higher proportion could be the possible reason for these broad peaks and the peak shift observed in the XRD patterns.

In this study, $[P(C_6H_{13})_3C_{14}H_{29}][FeCl_4]$ was utilized as a dual P and Fe source for *in situ* preparation of Fe_2P. Previous investigations have demonstrated that the quaternary phosphonium cation of an IL can decompose to a trialkylphosphine (TAP) and that the metal-based anion can be reduced to give metal nanoparticles (M–NPs).[30,31] This TAP, utilized as an organophosphine to prepare transition metal phosphides (TMPs), can exhibit a strong coordination interaction with the M–NPs to form a complex, such as Ni–TAP or Co–TAP.[32,33] In this case, Fe–TAP was generated during the pyrolysis step and the P–C bond could be broken to form phosphorus. Finally, the metal and phosphorus react to obtain the TMP.[5] Accordingly, the possible synthetic route for Fe_2P using $[P(C_6H_{13})_3C_{14}H_{29}][FeCl_4]$ is described in Scheme 1. During the preparation, the IL can also be used as a solvent and a stabilizer to prevent the aggregation of the nanoparticles.[19,34] Furthermore, according to the TEM and SEM images of all four materials, $Fe_2P_{(IL6)}$ is a large bulky material on the micrometer scale while the other three catalysts with CNTs are on the nanometer scale. Thus, the CNTs are favorable for the formation of iron phosphide nanoparticles by dispersing the IL and avoiding aggregation.

The HER activities of $Fe_2P_{(IL6)}$/CNTs and $Fe_2P_{(IL4)}$/CNTs were studied. $Fe_2P_{(IL6)}$ and FeP/CNTs, pyrolyzed from $[P(C_6H_{13})_3C_{14}H_{29}][FeCl_4]$ and $FeCl_3 \cdot 6H_2O$/CNTs/NaH_2PO_2 respectively, were introduced as control groups. As shown in Fig. 5a, $Fe_2P_{(IL6)}$/CNTs possesses the best HER activity, holding the lowest onset overpotential of 75 mV. It can also achieve current densities of 10 and 20 mA cm^{-2} at overpotentials of 115 and 150 mV, respectively. On the contrary, $Fe_2P_{(IL6)}$ displays a much lower activity than $Fe_2P_{(IL6)}$/CNTs and $Fe_2P_{(IL4)}$/CNTs. Thus, the CNTs played a pivotal role in improving the HER performance. It is highly possible that the CNTs can disperse the IL to small droplets, which is beneficial for forming the Fe_2P nanoparticles.

Tafel plots for these materials were investigated, and the corresponding Tafel slopes were calculated (Fig. 5b). The Tafel slope for $Fe_2P_{(IL6)}$ is higher than 120 mV dec^{-1}, suggesting that a Volmer step (proton adsorption) is the rate-limiting step.[35] On the contrary, the Tafel slope of $Fe_2P_{(IL6)}$/CNTs is the lowest (68 mV dec^{-1}), revealing that this process is a Volmer–Heyrovsky reaction and that the rate-limiting step is a Heyrovsky step (charge transfer step). Therefore, enhancing the conductivity and electron transfer ability of the material could significantly improve the catalytic activity of $Fe_2P_{(IL6)}$/CNTs. In addition, the low Tafel slope of $Fe_2P_{(IL6)}$/CNTs demonstrates good hydrogen evolution kinetics and a low energy barrier for H_2 electrochemical desorption.

Electrochemical Impedance Spectroscopy (EIS) analysis was conducted to further evaluate catalytic performance. As shown in Fig. 5c, $Fe_2P_{(IL6)}$/CNTs possesses the lowest faradaic impedance (~30 Ω) while $Fe_2P_{(IL6)}$ has a much higher impedance. This demonstrates that $Fe_2P_{(IL6)}$/CNTs possesses a high electrical conductivity and good electron transfer ability which, given that charge transfer is the rate-limiting step for this catalyst, can

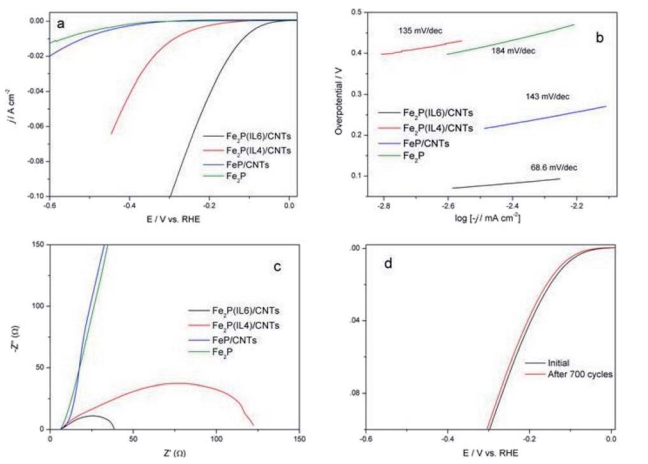

Fig. 5 (a) Linear sweep voltammograms at the working electrode using the four materials; (b) Tafel plots for the HER using the four materials; and (c) electrochemical impedance spectroscopy data for the four materials. Data were collected for the electrode at a HER overpotential of 370 mV; $Fe_2P_{(IL6)}$/CNTs (black), $Fe_2P_{(IL4)}$/CNTs (red), FeP/CNTs (blue), and Fe_2P (green). (d) Linear sweep voltammograms at the working electrode using $Fe_2P_{(IL6)}$/CNTs; initial trial: black, trial after 700 scanning cycles: red. Catalyst loading: 50 μg. Electrolyte: 0.5 M H_2SO_4. IL to CNTs ratio: 5 : 1.

dramatically improve the catalytic activity. Thus, it is worth noting that the CNTs can not only facilitate the fabrication of the Fe_2P nanoparticles, but also improve the HER performance.

Additionally, both $Fe_2P_{(IL6)}$/CNTs and $Fe_2P_{(IL4)}$/CNTs have a better HER performance than FeP/CNTs, showing that the IL can improve HER activity (Table 1). The possible reason could be the carbonization of the IL cation during pyrolysis, which increases the electrical conductivity of the materials.[16] Also, the EDS results indicate that $Fe_2P_{(IL6)}$/CNTs and $Fe_2P_{(IL4)}$/CNTs have a higher iron phosphide content than that of FeP/CNTs, improving the HER performance.

When compared with $[P(C_4H_9)_4][FeCl_4]$ (colloidal solid), $P(C_6H_{13})_3C_{14}H_{29}][FeCl_4]$ (liquid) is more convenient to mix with the CNTs, forming smaller IL droplets that subsequently generate smaller Fe_2P particles. Brunauer–Emmett–Teller (BET) measurements were carried out. $Fe_2P_{(IL6)}$/CNTs has a higher surface area (163 $m^2\ g^{-1}$) than that of $Fe_2P_{(IL4)}$/CNTs (145 $m^2\ g^{-1}$), which can expose more active sites to enhance the HER activity.[36] These BET results also suggest that $Fe_2P_{(IL6)}$/CNTs has a smaller particle size than $Fe_2P_{(IL4)}$/CNTs, resulting in better HER performance. Moreover, the EDS analysis indicates that $Fe_2P_{(IL6)}$/CNTs has a higher Fe_2P content than $Fe_2P_{(IL4)}$/CNTs (Fig. 2b and S4†), which could be another reason for the better HER performance.

The stability of $Fe_2P_{(IL6)}$/CNTs in the HER was evaluated, and cyclic voltammetry (CV) over 700 scanning cycles was performed at the scan rate of 100 mV s^{-1}. After scanning, no significant change in the LSV was observed, indicating that this catalyst possesses a good cycle life during the HER (Fig. 4d). Therefore, $Fe_2P_{(IL6)}$/CNTs can serve as an effective and stable HER electrocatalyst, and its catalytic activity is comparable to other TMP catalysts used for the HER (Table 1). Moreover, $Fe_2P_{(IL6)}$ was prepared *in situ* on CNTs using the IL as a dual source of Fe and P, which is simple, fast and green and does not require the addition of other reagents.

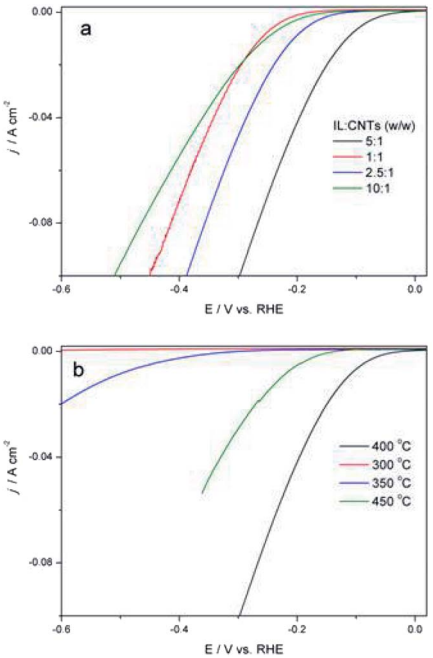

Fig. 6 (a) Linear sweep voltammograms at the working electrode using $Fe_2P_{(IL6)}$/CNTs where different IL/CNTs ratios were used to prepare the catalyst; IL : CNTs = 1 : 1 (red), IL : CNTs = 2.5 : 1 (blue), IL : CNTs = 5 : 1 (black), and IL : CNTs = 10 : 1 (green). (b) Linear sweep voltammograms at the working electrode using $Fe_2P_{(IL6)}$/CNTs where different pyrolysis temperatures were used to prepare the catalyst: 300 °C (red), 350 °C (blue), 400 °C (black), and 450 °C (green). Catalyst loading: 100 μg. Electrolyte: 0.5 M H_2SO_4.

The IL/CNTs ratio and pyrolysis temperature for $Fe_2P_{(IL6)}$/CNTs preparation were optimized. The IL to CNTs ratio was varied from 1 : 1 to 10 : 1, and the best ratio was 5 : 1 (Fig. 6a). It is possible that a high ratio of IL to CNTs could produce more $Fe_2P_{(IL6)}$ particles on the CNTs, while excess IL would form extra

Table 1 A comparison of the HER performance of $Fe_2P_{(IL6)}$/CNTs with other HER electrocatalysts

Catalyst	Onset overpotential (mV)	Tafel slope (mV dec^{-1})	j (mA cm^{-2})	η at the corresponding j (mV)	Ref.
Fe_2P(IL6)/CNTs	75	68	10	115	This work
			20	150	
Fe_2P(IL4)CNTs	120	130	10	290	
			20	340	
FeP/CNTs	350	143	10	520	
			20	600	
Fe_2P	350	184	10	570	
FeP/C	63	57	10	110	8
			20	147	
FeP NPs	85	64	10	124	16
FeP NPs/graphene	65	67	10	123	37
FeP NP-candle soot	38	58	10	112	38
FeP hollow microsphere	—	58	10	114	39
FeP and Fe_2P nanowires	50	39	10	96	25
FeP nanorods	150	55	10	120	40
3D-graphene aerogel CoP	—	50	10	121	41
MoP_2 nanosheets	90	81.5	10	150	9
Ni_2P nanoparticles	75	46	10	102	19

$Fe_2P_{(IL6)}$ that deteriorates the HER performance. Next, the pyrolysis temperature was increased from 300 to 500 °C (Fig. 6b), which is, depending on the iron and phosphorus precursors, the most suitable temperature range for preparing iron phosphide.[12–17] In this study, pyrolysis at too low a temperature will not obtain the final product, while too high a temperature will waste energy and increase the annealing time. Thus, 400 °C was used for phosphidation.

Conclusions

$Fe_2P_{(IL6)}$/CNTs was successfully prepared from $[P(C_6H_{13})_3C_{14}H_{29}][FeCl_4]$/CNTs, where $[P(C_6H_{13})_3C_{14}H_{29}][FeCl_4]$ was used as the dual source of Fe and P to fabricate Fe_2P for the first time. $Fe_2P_{(IL6)}$/CNTs was then utilized as an electrocatalyst for the HER where it displayed good HER activity and stability. CNTs not only improve the catalytic activity but are also favorable for the preparation of the Fe_2P nanoparticles. Moreover, the IL-based *in situ* preparation is facile and eco-friendly and does not require the addition of any other reagent. This method possesses great promise for application in other electrochemical studies. Future studies will focus on the trapping of volatiles and using gas chromatography-mass spectrometry (GC-MS) or other characterization methods to analyze the off-gases during the preparation process. This will be applied to further investigate the phosphidation mechanism.

Conflicts of interest

There are no conflicts to declare.

Acknowledgements

This work is financially supported by the National Natural Science Foundation of China (No. 51909012) and "Fundamental Research Funds of the Central University" (XDJK2019C004).

References

1 A. B. Laursen, S. Kegnæs, S. Dahl and I. Chorkendorff, Molybdenum sulfides-efficient and viable materials for electro-and photoelectrocatalytic hydrogen evolution, *Energy Environ. Sci.*, 2012, **5**, 5577.
2 J. F. Callejas, C. G. Read, C. W. Roske, N. S. Lewis and R. E. Schaak, Synthesis, characterization, and properties of metal phosphide catalysts for the hydrogen-evolution reaction, *Chem. Mater.*, 2016, **28**, 6017.
3 H. Hambourger, M. Gervaldo, D. Svedruzic, P. W. King, D. Gust, M. Ghirardi, A. L. Moore and T. A. Moore, [FeFe]-Hydrogenase-catalyzed H_2 production in a photoelectrochemical biofuel cell, *J. Am. Chem. Soc.*, 2008, **130**, 2015.
4 P. F. B. D. Martins, P. P. Lopes, E. A. Ticianell, V. R. Stamenkovic, N. M. Markovic and D. Strmcnik, Hydrogen evolution reaction on copper: promoting water dissociation by tuning the surface oxophilicity, *Electrochem. Commun.*, 2019, **100**, 30.
5 Y. Shi and B. Zhang, Recent advances in transition metal phosphide nanomaterials: synthesis and applications in hydrogen evolution reaction, *Chem. Soc. Rev.*, 2016, **45**, 1529.
6 F. Wang, X. Yang, B. Dong, X. Yu, H. Xue and L. Feng, A FeP powder electrocatalyst for the hydrogen evolution reaction, *Electrochem. Commun.*, 2018, **92**, 33.
7 M. Wei, L. Yang, L. Wang, T. Liu, C. Liu, Y. Tang and S. Luo, *In situ* potentiostatic activation to optimize electrodeposited cobalt-phosphide electrocatalyst for highly efficient hydrogen evolution in alkaline media, *Chem. Phys. Lett.*, 2017, **681**, 90.
8 K. Xiong, L. Huang, Y. Gao, H. Zhang, Y. Zhuo, H. Shen, Y. Wang, L. Peng and Z. Wei, Formation of a thin-layer of nickel hydroxide on nickel phosphide nanopillars for hydrogen evolution, *Electrochem. Commun.*, 2018, **92**, 9.
9 Y. Gao, M. Zhang, J. Ding, S. Hong, J. Masa, S. Liu and Z. Sun, Simple synthesis of two-dimensional MoP_2 nanosheets for efficient electrocatalytic hydrogen evolution, *Electrochem. Commun.*, 2018, **97**, 27.
10 T. Li, D. Tang and C. M. Li, Microwave-assisted synthesis of cobalt phosphide using ionic liquid as Co and P dual-source for hydrogen evolution reaction, *Electrochim. Acta*, 2019, **295**, 1027.
11 J. Tian, Q. Liu, A. M. Asiri and X. Sun, Self-supported nanoporous cobalt phosphide nanowire arrays: an efficient 3D hydrogen-evolving cathode over the wide range of pH 0–14, *J. Am. Chem. Soc.*, 2014, **136**, 7587.
12 D. E. Schipper, Z. Zhao, A. P. Leitner, S. L. Donaldson, A. Kumar, F. Qin, Z. Wang, J. Bao, H. Thirumalai, L. C. Grabow and K. H. Whitmire, Effects of Catalyst Phase on the Hydrogen Evolution Reaction of Water Splitting: Preparation of Phase-Pure Films of FeP, Fe_2P, and Fe_3P and their Relative Catalytic Activities, *Chem. Mater.*, 2018, **30**, 3588.
13 Y. Park, H. Kang, Y.-K. Hong, G. Cho, M. Choi, J. Cho and D.-H. Ha, Influence of the phosphorus source on iron phosphide nanoparticle synthesis for hydrogen evolution reaction catalysis, *Int. J. Hydrogen Energy*, 2020, DOI: j.ijhydene.2020.03.051.
14 Z. Zhao, D. E. Schipper, A. P. Leitner, H. Thirumalai and J. Bao, Bifunctional metal phosphide FeMnP films from single source metal organic chemical vapor deposition for efficient overall water splitting, *Nano Energy*, 2017, **39**, 444.
15 E. Muthuswamy, P. R. Kharel, G. Lawes and S. L. Brock, Control of phase in phosphide nanoparticles produced by metal nanoparticle transformation: Fe_2P and FeP, *ACS Nano*, 2009, **3**, 2383.
16 G. Cho, H. Kim, Y. S. Park, Y. K. Hong and D. H. Ha, Phase transformation of iron phosphide nanoparticles for hydrogen evolution reaction electrocatalysis, *Int. J. Hydrogen Energy*, 2018, **43**, 11326.
17 A. T. Kelly, I. Rusakova, T. Ould-Ely, C. Hofmann, A. Lüttge and K. H. Whitmire, Iron phosphide nanostructures produced from a single-source organometallic precursor: nanorods, bundles, crosses, and spherulites, *Nano Lett.*, 2007, **7**, 2920.

18 B. Zhang, Y. Xue, A. Jiang, Z. Xue, Z. Li and J. Hao, Ionic liquid as reaction medium for synthesis of hierarchically structured one-dimensional MoO_2 for efficient hydrogen evolution, *ACS Appl. Mater. Interfaces*, 2017, **9**, 7217.

19 C. Zhang, B. Xin, Z. Xi, B. Zhang, Z. Li, H. Zhang, Z. Li and J. Hao, Phosphonium-based ionic liquid: a new phosphorus source toward microwave-driven synthesis of nickel phosphide for efficient hydrogen evolution reaction, *ACS Sustainable Chem. Eng.*, 2018, **6**, 1468.

20 T. Li, D. Tang and C. M. Li, A high active hydrogen evolution reaction electrocatalyst from ionic liquids-originated cobalt phosphide/carbon nanotubes, *Int. J. Hydrogen Energy*, 2017, **42**, 21786.

21 Z. Cui, T. Li, D. Tang and C. M. Li, Ionic liquids-based iron phosphide/carbon nanotubes composites: high active electrocatalysts towards hydrogen evolution reaction, *ChemistrySelect*, 2017, **2**, 1019.

22 N. Deng, M. Li, L. Zhao, C. Lu, S. L. D. Rooy and I. M. Warner, Highly efficient extraction of phenolic compounds by use of magnetic room temperature ionic liquids for environmental remediation, *J. Hazard. Mater.*, 2011, **192**, 1350.

23 J. Wang, Q. Yang and Z. Zhang, Selective Synthesis of magnetic Fe_2P/C and FeP/C core/shell nanocables, *J. Phys. Chem. Lett.*, 2010, **1**, 102.

24 Y. Yan, B. Zhao, S. Yi and X. Wang, Assembling pore-rich FeP nanorods on the CNT backbone as an advanced electrocatalyst for oxygen evolution, *J. Mater. Chem. A*, 2016, **4**, 13005.

25 C. Qian, F. Kim, L. Ma, F. Tsui, P. Yang and J. Liu, Solution-Phase synthesis of single-crystalline iron phosphide nanorods/nanowires, *J. Am. Chem. Soc.*, 2004, **126**, 1195.

26 C. Y. Son, I. H. Kwak, Y. R. Lim and J. Park, FeP and FeP_2 nanowires for efficient electrocatalytic hydrogen evolution reaction, *Chem. Commun.*, 2016, **52**, 2819.

27 F. Luo, H. Su, W. Song, Z. Wang, Z. Yuan and C. Yan, Magnetic and magnetotransport properties of Fe_2P nanocrystallites *via* a solvothermal route, *J. Mater. Chem.*, 2004, **14**, 111.

28 P. Jiang, Q. Liu, Y. Liang, J. Tian, A. M. Asiri and X. Sun, A cost-effective 3D hydrogen evolution cathode with exceptionally high catalytic activity: FeP nanowires array as the active phase, *Angew. Chem., Int. Ed.*, 2014, **53**, 12855.

29 E. J. Popczun, C. G. Read, C. W. Roske, N. S. Lewis and R. E. Schaak, A cost-effective 3D hydrogen evolution cathode with high catalytic activity: FeP nanowire array as the active phase, *Angew. Chem., Int. Ed.*, 2014, **53**, 5427.

30 C. Read, J. Callejas, C. Holder and R. Schaak, General strategy for the synthesis of transition metal phosphide films for electrocatalytic hydrogen and oxygen evolution, *ACS Appl. Mater. Interfaces*, 2016, **8**, 12798.

31 F. Liang, L. Huang, L. Tian, J. Li, H. Zhang and S. Zhang, Microwave-assisted hydrothermal synthesis of cobalt phosphide nanostructures for advanced supercapacitor electrodes, *CrystEngComm*, 2018, **20**, 2412.

32 Y. Pan, Y. Liu, J. Zhao, K. Yang, J. Liang, D. Liu, W. Hu, D. Liu, Y. Liu and C. Liu, Monodispersed nickel phosphide nanocrystals with different phases: synthesis, characterization and electrocatalytic properties for hydrogen evolution, *J. Mater. Chem. A*, 2015, **3**, 1656.

33 D. Tang, T. Li and C. M. Li, Metal and phosphonium-based ionic liquid: a new Co and P dual-source for synthesis of cobalt phosphide toward hydrogen evolution reaction, *Int. J. Hydrogen Energy*, 2019, **44**, 1720.

34 R. Welton, Room temperature ionic liquids. Solvents for synthesis and catalysis, *Chem. Rev.*, 1999, **99**, 2071.

35 B. E. Conway and B. V. Tilak, Interfacial processes involving electrocatalytic evolution and oxidation of H_2, and the role of chemisorbed H, *Electrochim. Acta*, 2002, **47**, 3571.

36 J. Wang, F. Xu, H. Jin, Y. Chen and Y. Wang, Non-noble metal-based carbon composites in hydrogen evolution reaction: fundamentals to applications, *Adv. Mater.*, 2017, **29**, 1605838.

37 Z. Zhang, B. Lu, J. Hao, W. Yang and J. Tang, FeP nanoparticles grown on graphene sheets as highly active non-precious-metal electrocatalysts for hydrogen evolution reaction, *Chem. Commun.*, 2014, **50**, 11554.

38 Z. Zhang, J. Hao, W. Yang, B. Lu and J. Tang, Modifying candle soot with FeP nanoparticles into high-performance and cost-effective catalysts for the electrocatalytic hydrogen evolution reaction, *Nanoscale*, 2015, **7**, 4400.

39 X. Guo, Z. Feng, Z. Lv, Y. Bu, Q. Liu, L. Zhao, C. Hao, G. Li and Q. Lei, Formation of uniform FeP hollow microspheres assembled by nanosheets for efficient hydrogen evolution reaction, *ChemElectroChem*, 2017, **4**, 2052.

40 H. Du, S. Gu, R. Liu and C. M. Li, Highly active and inexpensive iron phosphide nanorods electrocatalyst towards hydrogen evolution reaction, *Int. J. Hydrogen Energy*, 2015, **40**, 14272.

41 X. Zhang, Y. Han, L. Huang and S. Dong, 3D graphene aerogels decorated with cobalt phosphide nanoparticles as electrocatalysts for the hydrogen evolution reaction, *ChemSusChem*, 2016, **9**, 3049.s.

